# Investigating the faulted performance of warship power systems with integrated energy storage

L Farrier[1] MEng MSc AMIMarEST

* *University College London, Department of Mechanical Engineering, London, UK*
* Corresponding Author Email: luke.farrier.14@ucl.ac.uk

**Synopsis**

The need to integrate energy storage systems (ESS) with warship power systems to meet future dynamic loads such as high power electric weapons is apparent. This opens up challenges with design integration of ESS with power systems and operational aspects such as steady-state, transient and faulted performance. This paper describes the integration of ESS with a candidate power system as a case study as part of an ongoing time-domain simulation investigation at University College London. The paper describes the models and power management structure of the simulation testbed, that comprises battery based ESS and diesel generators in a hybrid electric power and propulsion system. The results of two scenarios are presented, the first verifies power sharing between a diesel generator and ESS during load levelling under single generator operation, the second illustrates the ability of the ESS to provide ride through power during a generator fault on the main distribution bus. The conclusions suggest that under voltage in the candidate system outside of acceptable limits occurs during fault ride through when in single generator operation.

*Keywords: Energy storage, Integration, Power management*

## 1. Introduction

Increasing importance is being placed on warship electrical power systems to support future pulsed weapons and combat systems. This has imparted greater demands on warship power system performance, and the requirement to integrate electrical energy storage systems (ESS) to buffer the stochastic load profiles inherent in combat systems (Hebner *et al.* 2015). The benefits of their integration have been widely reported in the literature, from an operational perspective with fast response rates to load changes and increased fault resilience (Radan *et al.* 2016).

Whilst the integration of large scale ESS with warships is currently limited to rotating machines in the Electromagnetic Aircraft Launch System on the USS Gerald R. Ford. ESS are becoming a more prominent feature in commercial ship power systems (Stevens *et al.* 2017), notably since the offshore supply vessel, Viking Lady was tested with 450 kWh of Lithium-ion (Li-ion) based batteries in 2012 (Stefanatos *et al.* 2015). Arguably the adoption of Li-ion based ESS in the automotive and micro-grid sectors has paved the way for their use in the marine sector (Geertsma *et al.* 2017). The integration of ESS with warship electric power systems opens up a number of challenges under steady-state, transient and faulted operating conditions. The ability of ES to alleviate quality of power supply (QPS) concerns under transient scenarios have been extensively reported (Gattozzi *et al.* 2015, Whitelegg 2016, Vu, Gonsoulin, Diaz, *et al.* 2017) however the challenge of managing the power between sources under fault scenarios with a centralised ESS has potentially been limited.

When managed correctly, a centralised ESS could alleviate the inherent reliance on local dedicated uninterruptable power supplies, typical of the current generation of warships with electric propulsion (Tate and Rumney 2017). With regard to power management, Geertsma *et al.* (2017) extensively reviewed the control strategies for ship power and propulsion, highlighting the need for further research in the control of hybrid power supplies (ESS and conventional power generation). Vu *et al.* (2017) have reported on the use of energy management techniques to manage power sources in a warship DC distribution system, demonstrating the ability of a predictive control method to coordinate ESS and generator sets to meet the high ramp rate demands of an Electromagnetic Railgun.

---

**Author's Biography**

Luke Farrier is a Marine Engineering Research Assistant at UCL and 2nd year PhD student investigating power system performance when integrating energy storage systems. Prior to this he obtained a degree in Mechanical Engineering from the University of Exeter, after which he completed the graduate scheme with MoD Defence Equipment and Support where he obtained his MSc in Marine Engineering (Electrical) from UCL.

This paper, inspired by the aforementioned authors work and research in the automotive, land based micro-grid and commercial marine sector, focuses on the integration of ESS with a candidate naval power system with AC distribution as a case study. This paper will investigate the power sharing between diesel generators (DGs and ESS in the candidate system under firstly under dynamic load and secondly, during a faulted condition. The work presented is part of an ongoing investigation using simulation-based research at University College London into ESS characterisation, and power management between battery ESS and DGs in a hybrid electric power and propulsion system.

## 2. Energy storage integration case study

### *2.1. Candidate ship power system*

The candidate naval ship power and propulsion system is akin to the CODLOG topology as described by McNaughtan *et al.* (2016). The ship particulars, power speed curve and equipment ratings were selected based on the work of Gemmell et al. (2014) and generic ASW operating profile derived from Partridge and Thorp (2014), both summarised in Appendix 1. The power and propulsion system (Figure 1) incorporates 4 x 2.83 MW diesel generators (DGs) as the primary source of power connected to two main switchboards rated at 690 V. Two feeders supply the ship service switchboards via 690/440 V step-down transformers. Integrated with the power and propulsion system is a Li-ion based battery ESS system connected to the distribution system via a bi-directional three-level converter, link impedance, 11$^{th}$ harmonic tuned filter and delta wye transformer, the latter providing galvanic isolation and preventing the penetration of zero sequence harmonics to the distribution system.

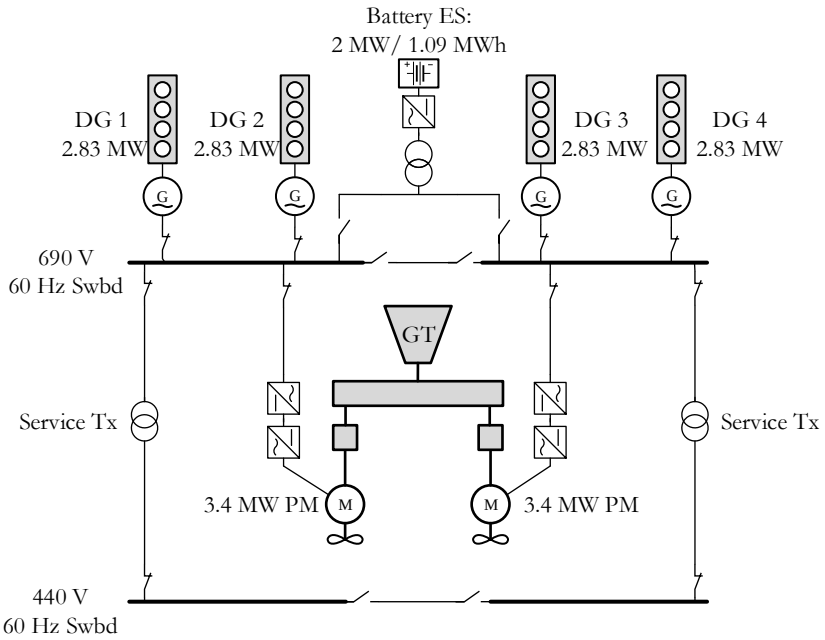


Figure 1: Candidate ship power and propulsion system

### *2.2. Scenario 1: load levelling*

The aim of this scenario is to demonstrate the ability of the ESS and one DG to operate in parallel, sharing power in a stable manner under quasi-steady state conditions. The first case study involves holding DG 1 at a constant loading condition of 75% Maximum Continuous Rating (MCR), whilst the ESS compensates for fluctuating power demand on the distribution bus. This facilitates the prime mover to operate within its most efficient envelope, as the DG speed governor is held constant i.e. the fuel injection rate is constant.

### *2.3. Scenario 2: Generator fault ride through*

The aim of this scenario is to demonstrate the ability of the ESS to provide continuity of power supply to the distribution bus following a generator fault, whilst maintaining QPS to consumers. Thus allowing the investigation of the transient and faulted impact on the ship distribution system. The ESS sizing requirement for the candidate ship was set to be able to provide 2 MW of power for a period of 10 minutes when cruising at 10

knots in electric propulsion mode with 2.5 MW temperate hotel load, the latter load based the work of Gemmell *et al.* (2014). This sets a minimum ESS energy requirement of 0.33 MWh. The speed selected as the ship is assumed to operate for 70% of its operating profile at this speed or lower per year (Appendix 1). The scenario investigated in this work is a fault ride through during single generator operation, in a low power state.

### *2.4. Constraints and assumptions*

To provide operational context to each scenario the following constraints and assumptions were made:

1. For each scenario it was assumed that the DG can be nominally loaded up to 85% MCR allowing sufficient margin to start another DG if the ES reserves are depleted or the ES is at maximum discharge power.

2. The ship was assumed to be operating in peacetime conditions, therefore the interconnector between the main switchboards was assumed closed, as a high level of resilience was not essential.

3. No load-shed logic was included during the fault ride through scenario so as to demonstrate the ability of the ES to provide continuity of power supply.

### *2.5. Battery energy storage characterisation*

The ESS consists of battery modules comprising Lithium Iron Phosphate (LFP) cells (Saft 2017), 18 modules connected in series form a string with nominal voltage rating of 830 V. The cell chemistry was considered appropriate owing to the balance offered between performance and safety. LFP cells are potentially more safe than alternative options due to a relatively high thermal runaway temperature and resilience to temperature fluctuations (Chemali *et al.* 2016, DNV GL 2016).

Of the two scenarios, the ride through power requirement is the most onerous, subsequently driving the characteristics of the ESS. For ESS sizing purposes it was assumed that the peak discharge rate is three times the nominal current rating (C-rate) during ride through and secondly that the State of Charge (SoC) of the battery system was limited to between 90% and 20% under normal operating conditions (Breucker *et al.* 2009, Wilson *et al.* 2017). Thereby avoiding regular high rate discharge to significant depths of discharge, therefore ensuring the preservation of battery life. Subsequently the ESS comprises 16 strings to provide a rated energy capacity of 1.09 MWh, that can deliver a maximum power output of 2 MW. The discharge power is limited by the voltage level of the battery, and subsequent current limits of the primary side of the transformer and IGBT power electronic devices in the converter.

## 3. Modelling

To investigate the power management and faulted performance when operating DGs and ESS in parallel during the two previously described scenarios, a simulation testbed was developed in MATLAB/Simulink, outlined by Figure 2. The constituent parts of the model are described in the following sections.

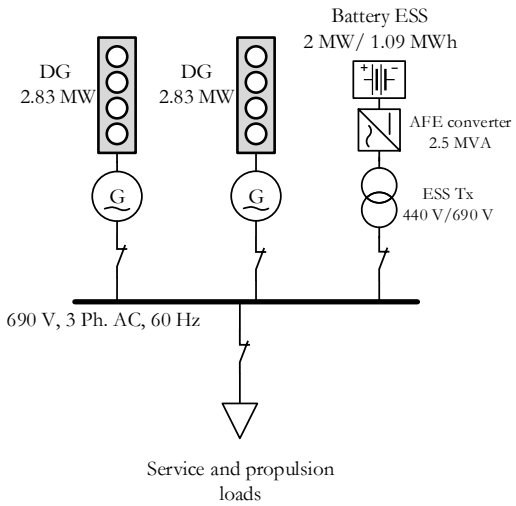

Figure 2: Simulation testbed

### *3.1. Diesel generator set*

The DG model consists of the diesel engine and governor, synchronous machine and an IEEE Type 2 AVR (Figure 3). The diesel engine model is derived from Yeager and Willis (1993), who validated its use against an emergency DG set, the parameters of the engine employed in this work are commensurate with Kanellos *et al.* (2007), who investigated voltage and frequency modulation under pulsed loads. The synchronous machine was modelled using a direct (d) and quadrature (q) representation, the parameters based on a machine of equivalent of power, voltage and frequency rating as provided by Cummins Generator Technologies (AvK-Alternators 2014). To ensure the model produced credible results, the AVR was tested against Lloyd's Register generator control testing procedure (Lloyd's Register 2017) in a similar manner to Whitelegg *et al.* (2015), results are provided in Appendix 2.

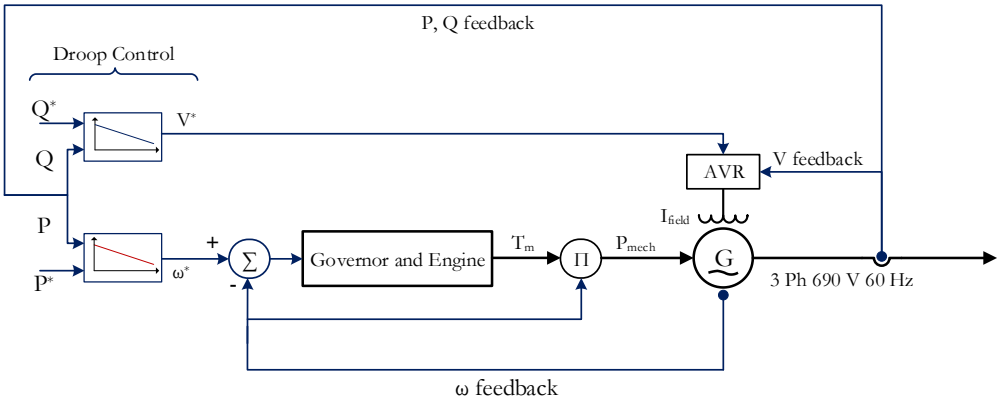


Figure 3: Diesel generator model schematic

### *3.2. Battery*

The battery strings described in section 2.5 were represented using Shepherd's model with lumped parameters, this was suitable as the investigation focused on power sharing among sources at the system level, and not the specific inter-cell dynamics. The battery model (Figure 4) consists of a controlled voltage source and internal resistance representative of the battery string arrangement, the internal resistance is assumed constant during charge and discharge (Mousavi and Nikdel 2014).

To verify the battery model, the response of a single battery module at 1 C discharge rate was verified against results provided by Saft (2017), the verification results are in Appendix 2. The module characteristics were then scaled to represent the whole battery system.

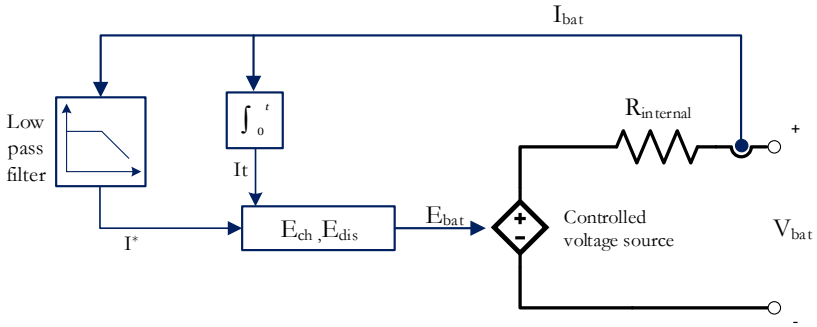


Figure 4: Battery model schematic

### *3.3. Converter, harmonic filter and transformer*

The battery feeds the distribution system via a three-level neutral point-clamped bi-directional converter comprising IGBT power electronic devices, rated at 2.5 MVA with a switching frequency of 2 kHz. The power converter is controlled as a voltage source grid-supporting converter, the implication being that the converter does not need an external reference to stay synchronised, therefore the ESS can provide ride through power and act as the sole power source if required.

The local control of the converter regulates the output voltage whilst controlling the current, and subsequently the battery charging and discharging. The local control comprises two cascade control loops comprising PI controllers, the outer accountable for voltage, the inner for current including feed-forward and decoupling network. The PI parameters were determined using *Ziegler-Nichols* (Fadali and Visioli 2013). Figure 5 shows the primary control implementation of the converter with frequency and voltage droop. Droop control is discussed further in section 3.4.

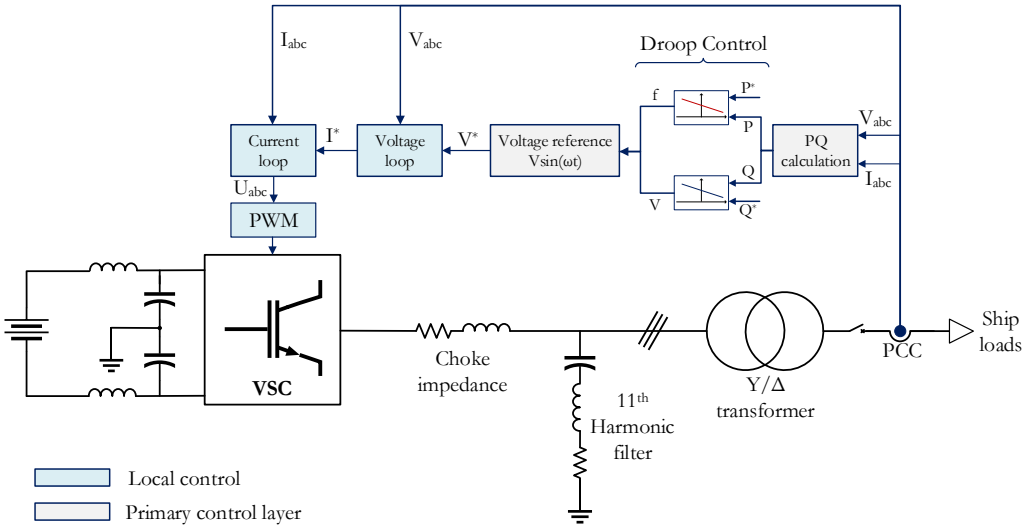


Figure 5: Converter model primary control with frequency and voltage droop

The sinusoidal current and voltage measurements at the point of common coupling (PCC) are transformed to dc components in the synchronous dq reference frame rotating at the measured distribution bus frequency. Control in the dq reference frame permits independent regulation of instantaneous real and reactive power using the following relationships:

$$P_t = \frac{3}{2}(v_d i_d + v_q i_q) \tag{1}$$

$$Q_t = \frac{3}{2}(-v_d i_q + v_q i_d) \tag{2}$$

Where, $P_t$ and $Q_t$ are the instantaneous real and reactive power, $v_d$ and $i_d$ are the output voltage and current in the d-axis, $v_q$ and $i_q$ donate the values in the q-axis. The converter is a twelve pulse device, therefore the dominant harmonics are the 11th and 13th, as a consequence the filter aims to attenuate the 11th harmonic. It was assumed that the distribution bus has a frequency tolerance of $\pm$3% as under NATO STANAG 1008 (NATO 2004), thus the bandwidth of the filter is 660 Hz $\pm$3%, rated at 250 kVAr, 10% of the nominal converter rating, with a tuning factor, $\delta$ of 0.23.

The transformer stepping up the output of the converter is rated to supply the maximum allowable power of the battery, 2 MW. A nominal power factor of 0.8 was assumed, therefore the transformer was rated at 2.5 MVA. The intrinsic line impedance of the transformer provides additional harmonic attenuation.

### *3.4. Control of the ship micro-grid*

As shown in Figure 6, the system control is hierarchical in three layers, supplementing the local control described above that regulates the voltage, frequency, real and reactive power at the output of the DG or ESS connected to the distribution bus. The distributed control architecture is influenced by the work of Guerrero *et al.* (2013) on land based micro-grids.

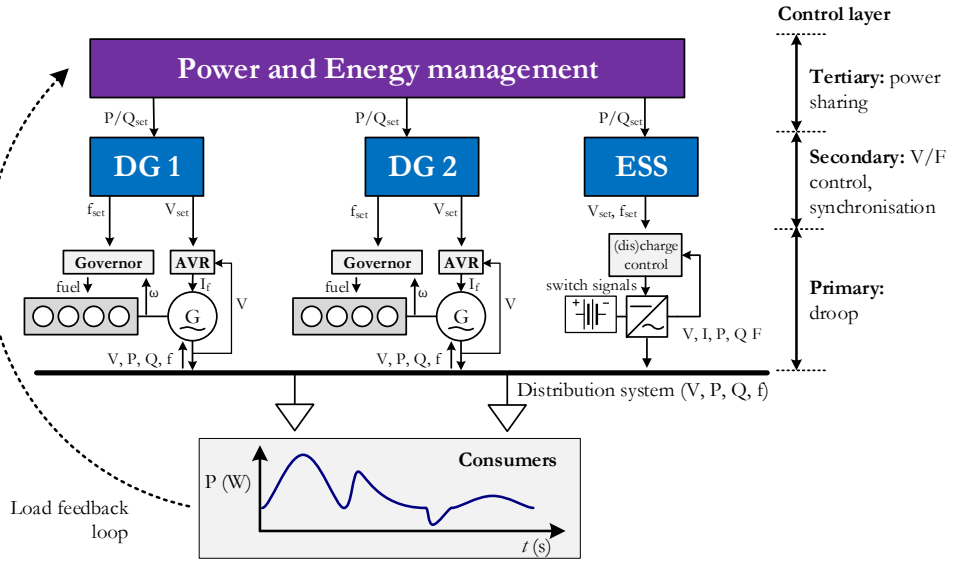


Figure 6: Hierarchical control levels of the simulation testbed

### *3.4.1. Primary layer*

The primary control layer adjusts the voltage and frequency references to the local control of the DG and ESS. To prevent the circulation of real and reactive power in the system, a linear frequency and voltage droop characteristic is included. The droop characteristic reduces the output frequency and voltage as real and reactive power increases, expressed as:

$$f = f^* - m(P - P^*) \tag{3}$$

$$V = V^* - n(Q - Q^*) \tag{4}$$

Where $f$ and $V$ are the frequency and voltage amplitude of the output voltage reference, $f^*$ and $V^*$ are the no load output frequency and voltage. $P$ and $Q$ are the output real and reactive powers respectively, with $P^*$ and $Q^*$ the DG or ESS load set points. $m$ and $n$ correspond to the droop slopes for frequency and voltage. Figure 7 shows the droop relationship for the DG and ESS, note that the ESS is able to generate active power ($P > 0$) and store energy ($P < 0$), act as a capacitor to supply reactive power ($Q > 0$), or as an inductor to absorb reactive power ($Q < 0$). Droop slopes are typically up to 5% (DNV-GL 2015), in this work the frequency and voltage droop settings were 2% and 3% of the rated power output of the DG and inverter respectively.

### *3.4.2. Secondary layer*

The secondary layer ensures that the voltage and frequency of the bus is stabilised. Synchronisation offsets are added to the frequency and voltage set points in this layer until the magnitude, frequency and phase difference (measured using a phase locked loop) between the power source and the grid voltages are within defined limits, <5 V, <0.5 Hz and <2° respectively. When the synchronisation criteria are met and held for 2 s the breaker is instructed to close, allowing power sharing between sources.

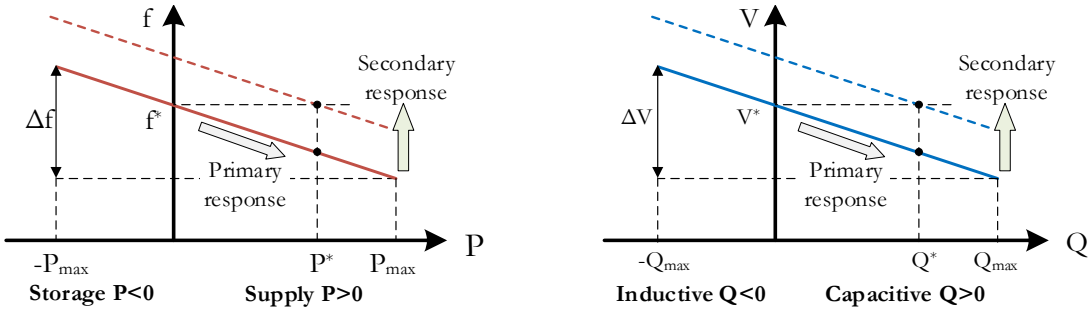


Figure 7: P-f and Q-V droop primary and secondary control relationships

*3.4.3. Tertiary control*

The tertiary layer is key to the scenario objectives described previously, as this manages the allocation of power to the DGs and ESS. The power management methodology in scenario 1 evaluates the real and reactive load demand at the distribution bus, allocating the demand to the DG or ESS whilst satisfying the following constraints:

$$\sum P_L = P_{DG} + P_{ESS} \tag{5}$$

$$0.5\ MCR \leq P_{DG} \leq 0.85\ MCR \tag{6}$$

Subject to

$$P_{Charge}^{Max} \leq P_{ESS} \leq P_{Discharge}^{Max} \tag{7}$$

Where $P_{DG}$, $P_{ESS}$ and $P_L$ are the DG, ESS and load real power, $P_{Charge}^{Max}$ and $P_{Discharge}^{Max}$ are the maximum charge and discharge power at 1C and 3C respectively. The power management strategy in scenario 2 maintains the constraints of scenario 1.

## 4. Simulation results

This paper aims to investigate the power sharing behaviour between DGs and ESS during dynamic load and faulted conditions. The results for both scenarios were generated using the model summarised in Figure 6.

### *4.1. Scenario 1: load levelling*

To share power in the AC system the output voltage of the ESS transformer and DG must be synchronised, this was achieved via a synchronisation control loop, the effectiveness of which is demonstrated in Figure 8. The plot shows the phase voltage synchronisation over time. The ESS is grid connected at 14s (Figure 8c) and sharing power with DG 1, this can be verified by the presence of harmonic distortion in the sinusoidal waveform. The total harmonic distortion was measured at 2% on the distribution bus under steady state conditions, ascertained using a Fast Fourier Transform of the waveform in Figure 8c.

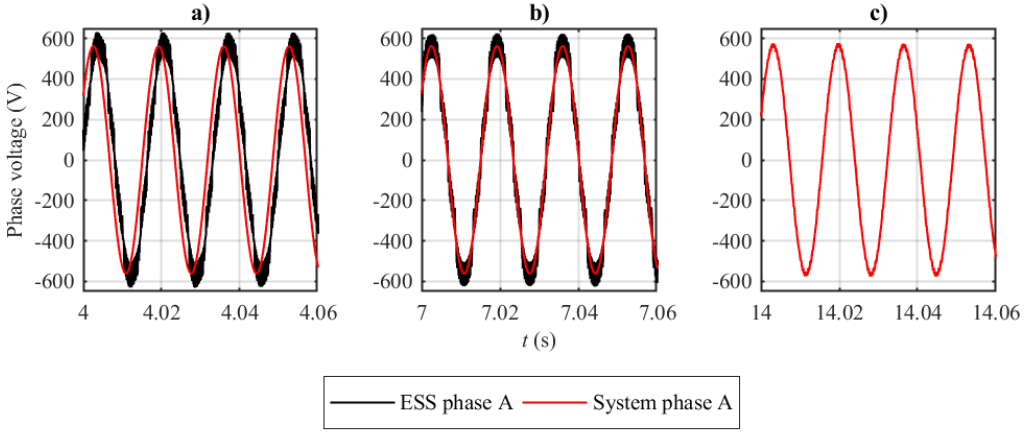


Figure 8: ESS output and system phase voltage a) prior to synchronisation b) during phase synchronisation and c) when the ESS is grid connected

The results in Figure 9a show the real power load demand of the ship varying with time, the speed governor of the DG is held constant resulting in constant power output of 75% MCR (2.13 MW). The exception occurs at Point A on Figure 9a where the load demand reaches 4.4 MW, during this load change the ESS reaches its discharge power limit of 2 MW, the discharge rate reflected in the state of charge plot in Figure 10. During this period, the power management layer increases the power set point of the DG to meet the excess load demand. Point B and C in Figure 9b show the effect of increasing and decreasing the DG power set point on system frequency. The linear P-f droop causes the system frequency to fall during increasing power output shown, and vice versa at 120 s. This is not evident during the load changes managed by the ESS likely due to the fast acting control loops of the inverter.

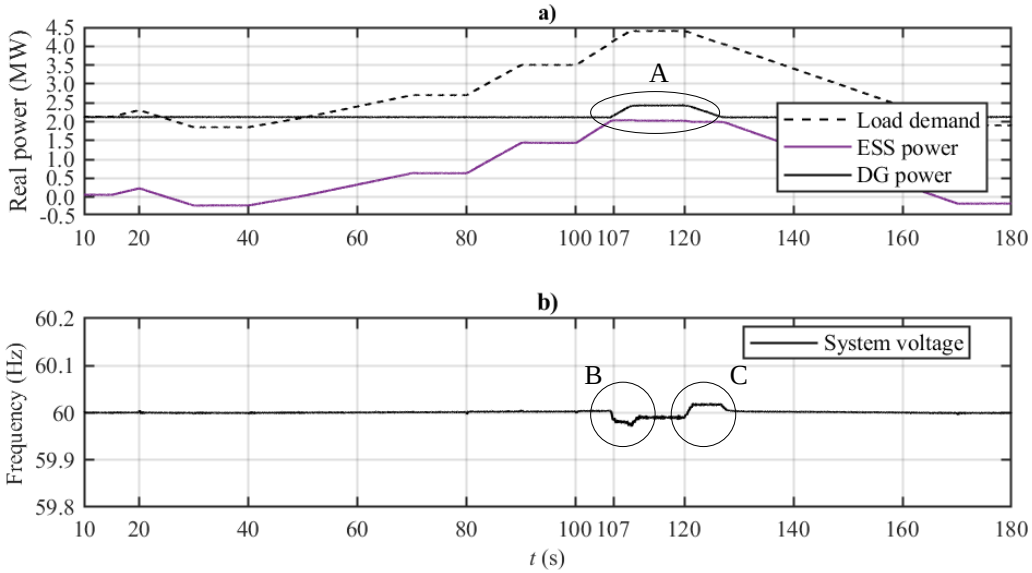

Figure 9: Simulation testbed a) real power and b) system frequency response during load levelling

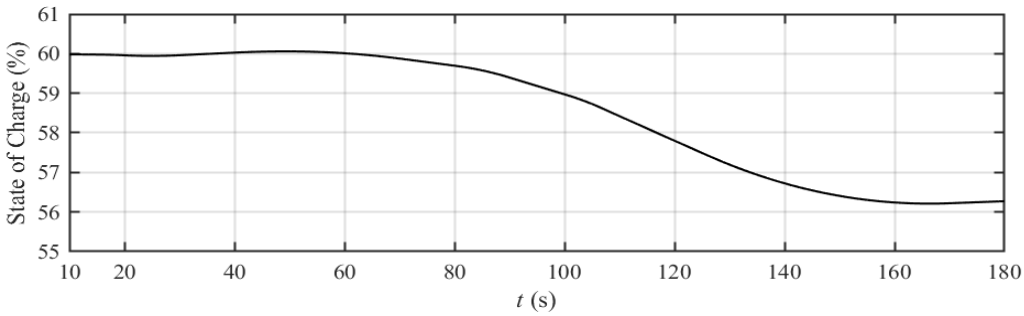

Figure 10: ESS state of charge during load levelling

The results in Figure 11a show how the reactive power of DG 1 and the ESS vary with time under the load-levelling scenario. Although the reactive power of the load in this scenario remains constant, the source reactive power supply is not constant, instead the reactive power supply varies with the real power load demand, when compared with Figure 9a. The consequence is that the voltage on the distribution bus, shown in Figure 11b, varies as a function of the real power load changes, converse to the frequency response where fluctuations are not evident.

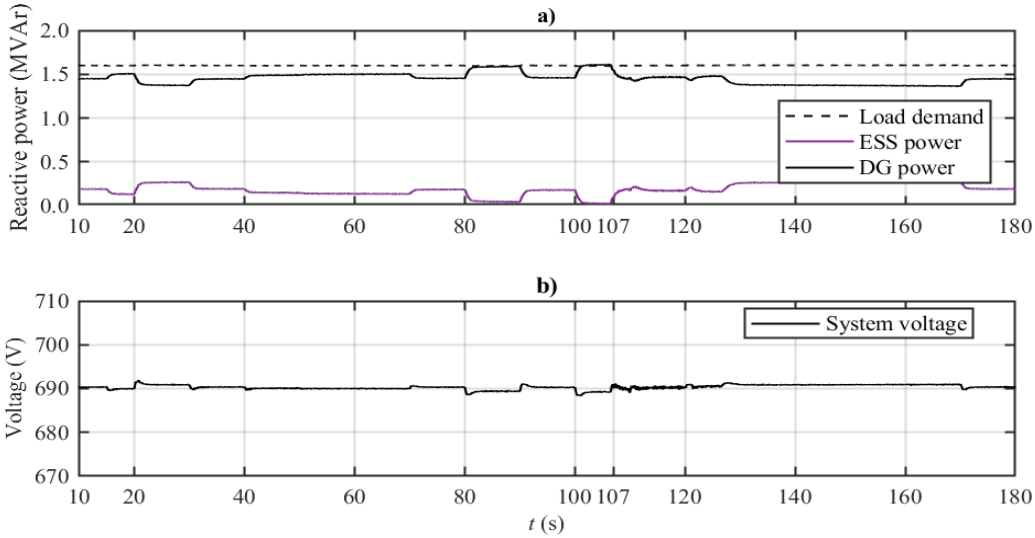

Figure 11: Model testbed a) reactive power and b) system voltage response to load changes during load levelling

The fluctuating reactive power between the DG and ESS can be explained by examining the governor and AVR relationships. Consider the synchronous generator real and reactive power equations (simplified considering that the armature winding resistance is small relative to the synchronous reactance, X);

$$P = \frac{VE}{X} sin\delta \tag{8}$$

$$Q = \frac{V}{X}(Ecos\delta - V) \tag{9}$$

Where $V$ is the terminal voltage of the generator, $E$ is the generator electromotive force (emf) and $\delta$ is the load angle (Prousalidis and Kourtesis 2013). The governor regulates speed slowly relative to the fast acting AVR, therefore from equation (8) the P-$\delta$ relationship considers the emf to be constant during real power load changes. Conversely the Q-V relationship from equation (9) senses changes in $\delta$ through cos $\delta$. Therefore, when the AVR senses change in voltage due to real power load change, the AVR reacts, adjusting the generator emf by controlling the field current and therefore reactive power, as shown by comparison of the simulation results in Figure 11 and Figure 12. When the generator load angle (Figure 12b) decreases due to increased real power demand, the AVR increases the field excitation current (Figure 12c) and therefore reactive power supplied by the generator.

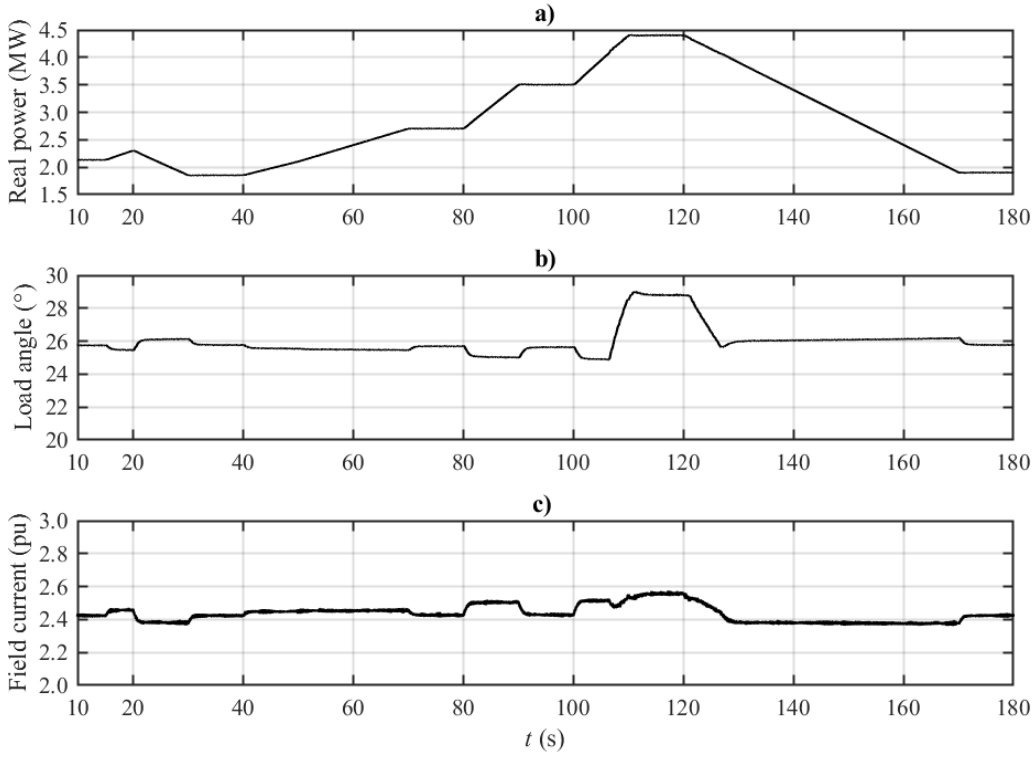


Figure 12: Simulation testbed a) real power load and DG 1 b) load angle and c) field excitation current during load levelling

### *4.2. Scenario 2: fault ride through*

The second scenario investigates the system behaviour during single generator operation mode, when a three phase to ground fault occurs across the terminals of the generator taking the generator offline. The scenario was used to assess the ability of the system to maintain quality and continuity of power following the fault. Prior to the fault DG 1 is operating at 75% MCR providing 2 MW of power to the ship and the excess power charging the battery, shown by the real power plotted in Figure 13a and magnified in Figure 13b. The fault is applied at 15 s shown by Point A. Immediately after the fault during the sub-transient phase, the current at the DG terminals rises and trips the overcurrent relay following a delay of approximately 30 ms. Prior to the trip, the ESS is injecting current into the fault, illustrated by Point B in Figure 13b. The trip signal causes the power management layer to

transfer the 2 MW load demand to the ESS, which is restored in approximately 1 s. Similarly, the reactive power drawn by the load is transferred to the ESS inverter following the fault. An increase in the reactive power of DG 1 occurs once the fault has cleared, this is likely attributed to the fault recovery period where the voltage of the generator rises therefore increasing the reactive power.

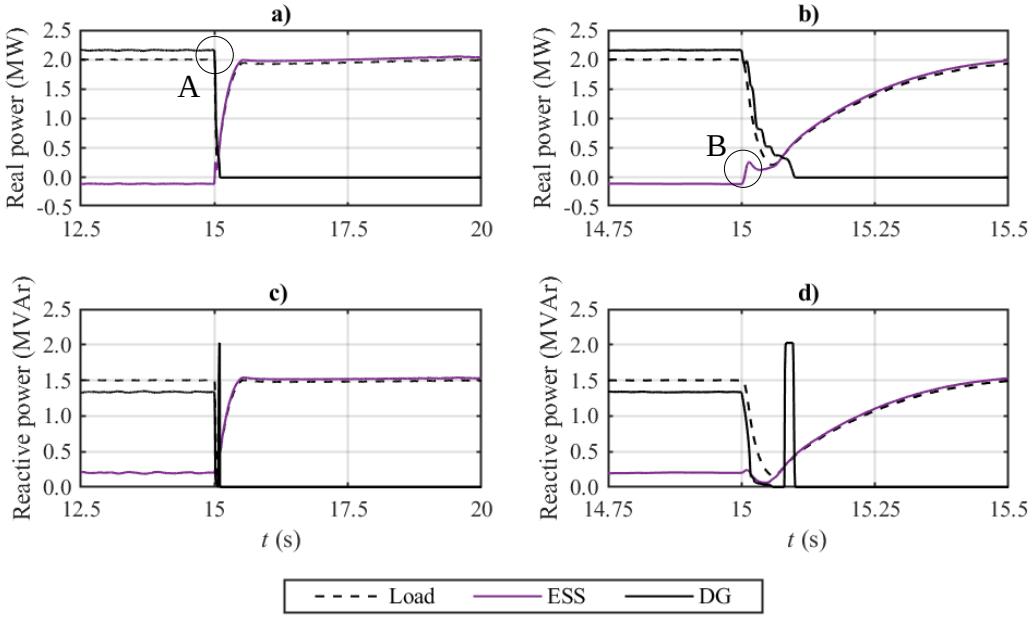


Figure 13: System a) and b) real power response, and c) and d) reactive power response to DG 1 fault

The voltage and frequency response to the fault are plotted in Figure 14. When the fault occurs the rms voltage of phase B and C dip to approximately 450 V (-35%), while phase A dips to 425 V, shown in Figure 14a. The asymmetric characteristic of the fault current means that the value of each phase voltage is different for ~50 ms after fault. The averaged rms voltage recovers to rated 690 V within 5 s. This excursion is outside the permitted transient tolerance limit for QPS standards (±20%). The system frequency during the fault, shown in Figure 14b, dips to 58.3 Hz (-3%), recovering within 5 s, this is within QPS limits. In reality it is likely that the under voltage condition would trigger protection relays, to either shed load or trip the ESS breaker on the 690 V secondary side of the transformer.

The extent of the excursions from rated voltage and frequency are dependent on the operating conditions at the time of fault, and in the examined case the synchronous machine is providing 75% of rated power and the ESS is being charged, therefore this is considered an extreme case.

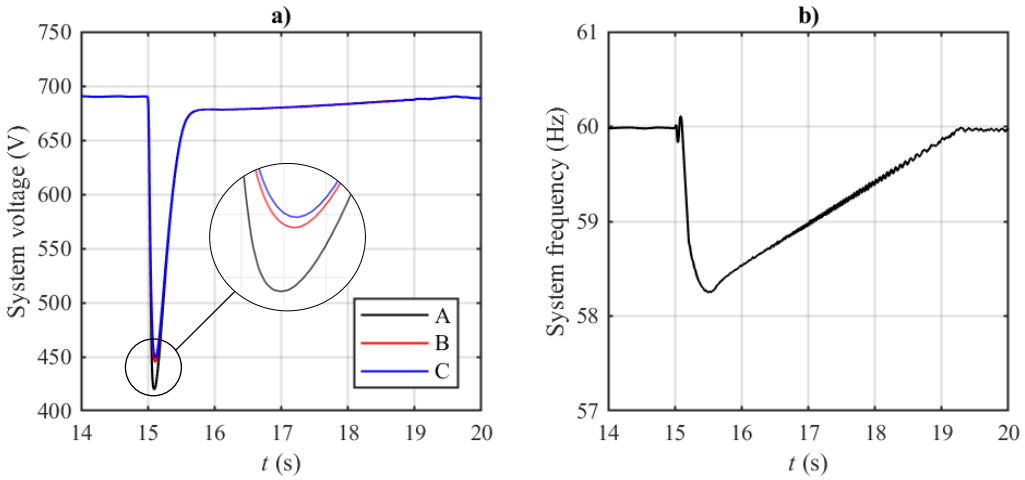


Figure 14: System a) rms voltage and b) frequency response to DG 1 fault

## 5. Conclusions and future work

The aim of this paper was to investigate the power sharing relationships between conventional diesel generator sets and energy storage systems under dynamic and faulted conditions. The presented work described the characterisation of a battery ESS to meet the requirements of two scenarios for a candidate warship power and propulsion system, prior to describing a power simulation testbed that is being used to investigate power management. The simulation results of the first scenario verified the ability of one DG and ESS to operate in parallel during dynamic conditions using a load-levelling case study. Secondly the results demonstrated the rapid response of the inverter control loops to maintain frequency under load changes. Finally, that unlike frequency, the system voltage, and therefore reactive power, varies under real power load changes during load levelling, caused by the AVR sensing changes in the generator load angle. To complete verification of the simulation testbed, scenario one will be expanded to include the second DG in future work.

The second scenario exhibited how an ESS can provide generator fault ride through power during single generator operation. The results of the simulation concluded that a peak of -35% under occurs, which is outside of acceptable QPS limits currently in place for warship power systems. Prior to the fault in this scenario, the DG is charging the ESS, this requires the ESS to rapidly transfer to discharging at maximum rated power to meet power system demand at the time of the fault. This contributes to the extent of under voltage. Future work will expand on scenario two presented here, and comprise varying the proportion of DG and ESS supply at the time of the generator fault in a sensitivity study to asses the implications on frequency and voltage deviations.

## 6. Acknowledgements

The support from Professor Richard Bucknall and the Marine Research Group at UCL in supervising this work is gratefully acknowledged.

## 7. References

AvK-Alternators, 2014. Technical Data Sheet for DSG 99 K0/4 AVK Alternator [online]. Available from: http://stamford-avk.com/products/AvK-alternator-range.

Breucker, S. De, Peeters, E., and Driesen, J., 2009. Possible applications of plug-in hybrid electric ships. *In*: *IEEE Electric Ship Technologies Symposium*. Baltimore, 310–317.

Chemali, E., Preindl, M., Malysz, P., and Emadi, A., 2016. Electrochemical and Electrostatic Energy Storage and Management Systems for Electric Drive Vehicles: State-of-the-Art Review and Future Trends. *IEEE Journal of Emerging and Selected Topics in Power Electronics*, 4 (3), 1117–1134.

DNV-GL, 2015. Part 3 Surface ships Chapter 2 Propulsion plants. *In*: *Rules for Classification of Naval Vessels*. DNV GL, 53–55.

DNV GL, 2016. DNV GL Handbook for Maritime and Offshore Battery Systems.

Fadali, M.S. and Visioli, A., 2013. *Digital Control Engineering - Analysis and Design*. 2nd ed. Elsevier.

Gattozzi, A.L., Herbst, J.D., Hebner, R.E., Blau, J.A., Cohn, K.R., Colson, W.B., Sylvester, J.E., and Woehrman, M.A., 2015. Power system and energy storage models for laser integration on naval platforms. *In*: *2015 EEE Electric Ship Technologies Symposium (ESTS 2015)*. Washington DC: IEEE, 173–180.

Geertsma, R.D., Negenborn, R.R., Visser, K., and Hopman, J.J., 2017. Design and control of hybrid power and propulsion systems for smart ships: A review of developments. *Applied Energy*, 194, 30–54.

Gemmell, G., McIntyre, B., and Reilly, M., 2014. Is IFEP a realistic future propulsion system for flexible frigates and destroyers? *In*: *International Naval Engineering Conference*. Amsterdam: IMarEST.

Guerrero, J.M., Chandorkar, M., Lee, T., and Loh, P.C., 2013. Advanced Control Architectures for Intelligent Microgrids; Part I: Decentralized and Hierarchical Control. *IEEE Transactions on Industrial Electronics*, 60 (4), 1254–1262.

Hebner, R.E., Davey, K., Herbst, J., Hall, D., Hahne, J., Surls, D.D., and Ouroua, A., 2015. Dynamic Load and Storage Integration. *Proceedings of the IEEE*, 103 (12), 2344–2354.

Kanellos, F., Hatzilau, I.K., and Prousalidis, J., 2007. Investigation of voltage/frequency modulation in ship electric networks with pulsed loads according to STANAG 1008 design constraints. *In*: *All Electric Ship (AES) 2007 The Vision Redrawn*. London: IMarEST.

Lloyd's Register, 2017. Vol 2, Part 9, Chapter 2, Electrical Power Generation and Energy Storage, 6.4 Generator control. *In*: *Rules and Regulations for the Classification of Naval Ships*. Lloyd's Register, 1033.

McNaughtan, N., McKinstry, G., and Wereski, R., 2016. De-risking strategy for the Type 26 Global Combat Ship electrical power and propulsion system. *In*: *International Naval Engineering Conference*. Bath: IMarEST.

Mousavi, S.M. and Nikdel, M., 2014. Various battery models for various simulation studies and applications. *Renewable and Sustainable Energy Reviews*, 32, 477–485.

NATO, 2004. *STANAG 1008 Characteristics of Shipboard Low Voltage Electrical Power Systems in Warships of the NATO Navies*. 9th ed. NATO Standardisation Agency.

Partridge, R. and Thorp, B.T., 2014. Re-writing the propulsion rule book for the 21st Century. *In*: *International Naval Engineering Conference*. Amsterdam: IMarEST.

Poirier, F. and D'Ussel, L., 2009. Lithium-ion battery technology- the most promising approach for exercise torpedoes [online]. Available from: https://www.saftbatteries.com/media-resources/knowledge-hub/white-papers.

Prousalidis, J.M. and Kourtesis, C.T., 2013. *Ship Electric Energy Systems: Design Operation Principles*. London: IMarEST.

Radan, D., Southall, M., Benatmane, M., and Butcher, M., 2016. Integration, optimisation and benefits of energy storage for marine applications. *In*: *International Naval Engineering Conference*. Bristol: IMarEST.

Saft, 2017. Seanergy® modules data sheet [online]. Available from: https://www.saftbatteries.com/products-solutions/products/seanergy-modules?text=&tech=88&market=&sort=newest&submit=Search.

Stefanatos, I.C., Dimopoulos, G.G., Kakalis, N.M.P., Vartdal, B., and Ovrum, E., 2015. Modelling and simulation of hybrid-electric propulsion systems : the Viking Lady case. *In*: *12th International Marine Design Conference*. Tokyo: The Japan Society of Naval Architects and Ocean Engineers, 161–178.

Stevens, J., Short, J., Mccarthy, J., Liu, X., and Wilson, G., 2017. Efficient power system design when incorporating Heavy Replenishment At Sea capability onto the Modern Naval Auxiliary Vessel. *In*: *Engine as A Weapon VII*. Bristol: IMarEST.

Tate, A. and Rumney, T., 2017. Taking the Dragon ( Fire ) to sea: UK MOD efforts to de-risk the integration of Laser DEW. *In*: *Engine as A Weapon VII*. Bristol: IMarEST.

Vu, T. V., Gonsoulin, D., Perkins, D., Diaz, F., Vahedi, H., and Edrington, C.S., 2017. Predictive energy management for MVDC all-electric ships. *In*: *2017 IEEE Electric Ship Technologies Symposium (ESTS 2017)*. Washington DC: IEEE, 327–331.

Vu, T. Van, Gonsoulin, D., Diaz, F., Edrington, C.S., and El-Mezyani, T., 2017. Predictive Control for Energy Management in Ship Power Systems Under High-Power Ramp Rate Loads. *IEEE Transactions on Energy Conversion*, 32 (2), 788–797.

Whitelegg, I., 2016. Power system design considerations when integrating electromagnetic railguns with electric warships. *In*: *International Naval Engineering Conference*. Bristol: IMarEST.

Whitelegg, I., Bucknall, R.W.G., and Thorp, B.T., 2015. On electric warship power system performance when meeting the energy requirements of electromagnetic railguns. *Journal of Marine Engineering & Technology*, 14 (2), 85–102.

Wilson, G., McCarthy, J., Xiong, J., Huan, Q., Venkatesh, P., Liu, X., and Tjandra, R., 2017. Use of Modelling and Simulation for Optimal Naval Ship Electrical System Design. *In*: *International Naval Engineering Conference*. Singapore: IMarEST.

Yeager, K.E. and Willis, J.R., 1993. Modeling of emergency diesel generators in an 800 megawatt nuclear power plant. *IEEE Transactions on Energy Conversion*, 8 (3), 433–441.

## 8. Appendix 1: Candidate ship characteristics

Table 1 details the candidate ship characteristics. Figure 15 details the operating profile based on Partridge and Thorp (2014) and power speed curve of the candidate ship derived from the ship characteristics, where power is the output power of the prime mover after losses. The DGs provide propulsion power to the electric motors up to 15 knots, above this speed the ship transitions from electric drive to GT drive, with the DGs supply the hotel and combat system loads only.

Table 1: Candidate ship characteristics (Gemmell *et al.* 2014)

| Ship Characteristic | Value |
|---|---|
| Displacement | 6,200 te |
| Length OA/LWL | 143/130 m |
| Beam OA | 17.2 m |
| Top speed | 29 kts |
| Economic speed | 12 kts |
| Hotel load | 2.5 MW |
| Shaft power at economic speed | 2.3 MW |

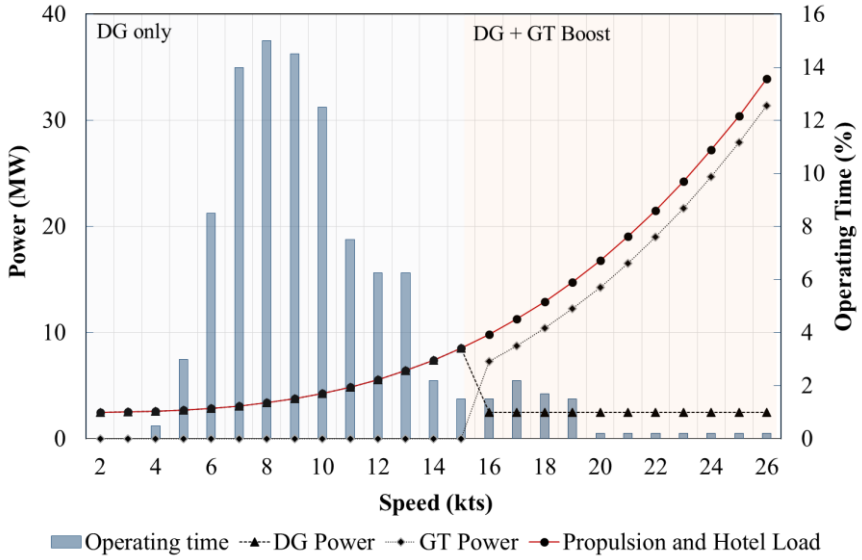


Figure 15: Candidate ship power speed curve and operating profile (Partridge and Thorp 2014)

## 9. Appendix 2: Parameters and verification results

### *9.1. ESS parameters*

Table 2: ESS parameters

| Parameter | Value |
|---|---|
| Modules per string | 18 |
| Number of strings | 16 |
| Capacity | 1.09 MWh |
| Nominal voltage | 831 V |
| Peak voltage | 957 V |
| Cut-off voltage | 680 V |
| Nominal discharge current (1C) | 1312 A |
| Peak continuous current | 3840 A |

### *9.2. DG verification results*

Table 3 details the AVR test procedure carried out in accordance with Lloyd's Register rules (Lloyd's Register 2017), corresponding results are shown in Figure 16 and Figure 17.

Table 3: AVR test procedure

| Description | Criteria | Measurement | Achieved? |
|---|---|---|---|
| 25% load | Voltage within ± 2.5% | 0.01% | Achieved |
| 50% load | Voltage within ± 2.5% | 0.01% | Achieved |
| 75% load | Voltage within ± 2.5% | 0.01% | Achieved |
| 100% load | Voltage within ± 2.5% | 0.01% | Achieved |
| 25% load – reject 25% load at 0.8 pf | Transient voltage rise <7.5% of rated voltage | 3.91% | Achieved |
| 50% load – reject 25% load at 0.8 pf | Transient voltage rise <7.5% of rated voltage | 4.03% | Achieved |
| 75% load – reject 25% load at 0.8 pf | Transient voltage rise <7.5% of rated voltage | 4.10% | Achieved |
| 100% load – reject 25% load at 0.8 pf | Transient voltage rise <7.5% of rated voltage | 4.16% | Achieved |

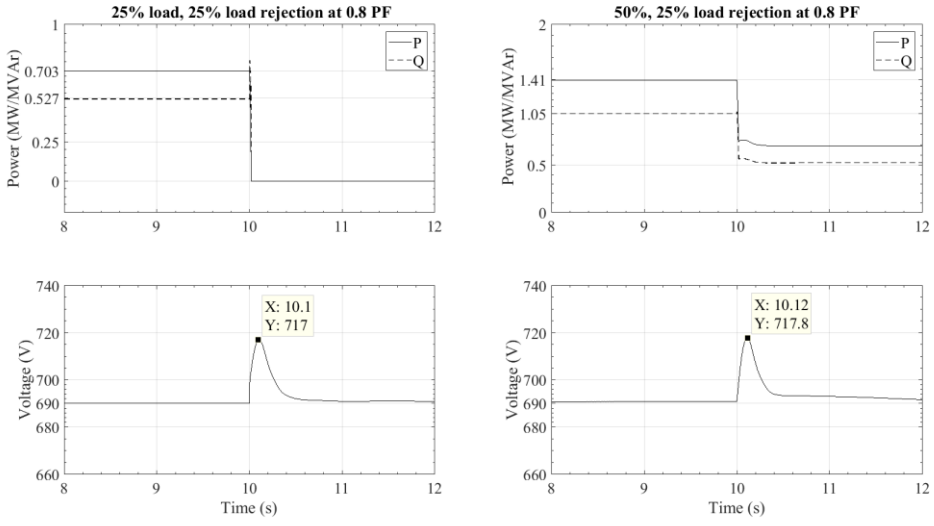


Figure 16: DG AVR test 5 and 6 results

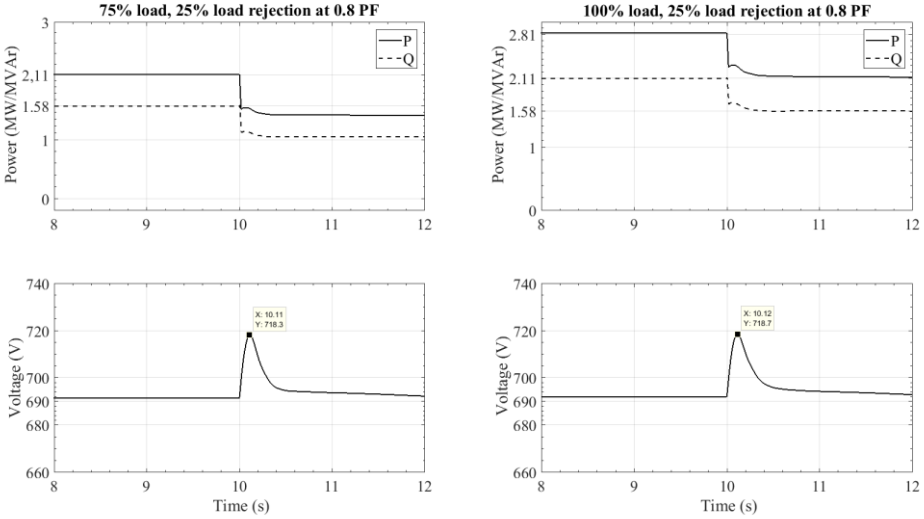


Figure 17: DG AVR test 7 and 8 results

### *9.3. Battery verification results at 1 C*

Battery module verification results are shown in Figure 18. The equivalent internal resistance of the modules are 0.098 Ω (Poirier and D'Ussel 2009). The region between 15% and 90% SOC of the module is the model confidence region. The error in this region is attributed to the internal resistance during the discharge cycle, assumed as constant, which is the same for charging.

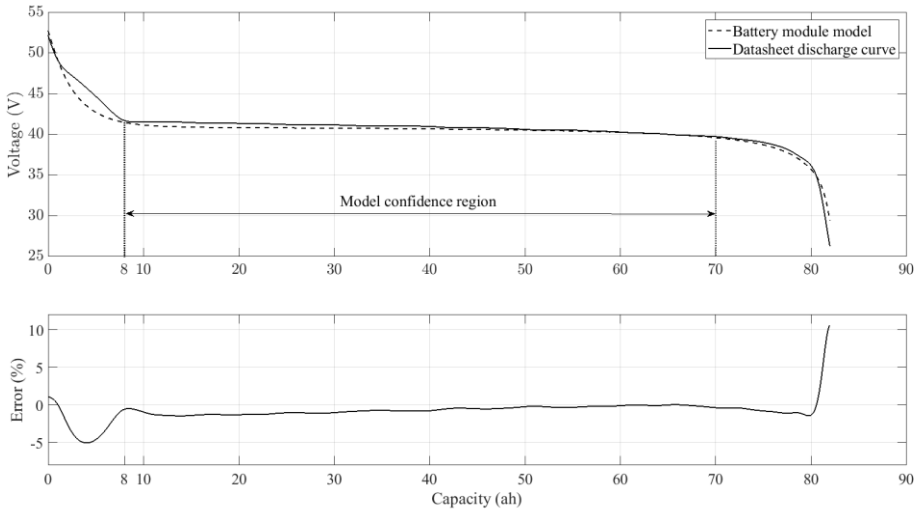


Figure 18: Battery module discharge comparison at 1 C